Tsunami generation by potential, partially submerged rockslides in an abandoned open-pit mine: The case of Black Lake, Québec, Canada

Jonathan Leblanc, Dominique Turmel, Jacques Locat, Carl B. Harbitz, Finn Løvholt, Jihwan Kim, Martin Grenon, and Ariane Locat

J. Leblanc, D. Turmel and J. Locat. Département de géologie et de génie géologique, Université Laval, Pavillon Adrien-Pouliot, 1065, avenue de la Médecine, Québec, QC, G1V 0A6, Canada.

C. B. Harbitz. , Løvholt, F., Kim, J. M., Norwegian Geotechnical Institute, P. O. Box. 3930, Ullevål Stadion, N-0806 Oslo, Norway.

M. Grenon. Département de génie des mines, de la métallurgie et des matériaux, Université Laval, Pavillon Adrien-Pouliot, 1065, avenue de la Médecine, Québec, QC, G1V 0A6, Canada.

A. Locat. Département de génie civil et de génie des eaux, Université Laval, Pavillon Adrien-Pouliot, 1065, avenue de la Médecine, Québec, QC, G1V 0A6, Canada.

Corresponding Author: Dominique Turmel (e-mail :dominique.turmel.1@ulaval.ca)

Abstract: The Black Lake rockslide is located on the east wall of an open pit mine initially operated by LAB Chrysotile near Thetford Mines, Québec. Movements were observed in July 2012 when a volume of 20 M m³ was mobilized, destroying a large portion of the Highway 112. Mining operations ceased in 2012, causing the complete shutdown of the pumping system whose goal was to prevent the rise of water level in the pit. As the water level increases in the pit, it is essential to determine the tsunamis generated by possible partially submerged rockslides and to understand their potential impacts. A series of possible scenarios have been analysed with regard to velocity and acceleration of the potential rockslide as well as the corresponding wave generation and inundation. Results from the simulation shows that when the factor of safety of the global slope is less than unity, inundation would not reach the potentially vulnerable infrastructures. Maximum wave height will vary as a function of the filling of the lake, and the lower wave height relative to water depth will happen when the lake will be completely filled.

Key words: Landslide-generated tsunami, partially submerged landslide, numerical modeling, open-pit mine, active rockslide.

Résumé : Le glissement de Black Lake est situé sur la paroi Est d'une ancienne mine à ciel ouvert exploitée par la compagnie LAB Chrysotile, à Thetford Mines, Québec. Ce glissement actif a connu un fort épisode de glissements en juillet 2012, où un volume de 20 M m³ a été mobilisé, emportant une large portion de la Route 112. Comme le niveau d'eau augmente dans la fosse en raison de l'arrêt des opérations minières, il devient primordial de déterminer le potentiel tsunamigénique des glissements de terrain possibles afin de comprendre le phénomène et de réagir efficacement à celui-ci. Plusieurs modélisations numériques ont été réalisées à partir de scénarios probables concernant le niveau de remplissage de la fosse ainsi que les vitesses et les accélérations de la masse dans le temps. Les modélisations effectuées ont permis de montrer que, lorsque le facteur de sécurité de la pente globale est inférieure à 1, aucune infrastructure ne pourrait être touchée par un éventuel tsunami. La hauteur maximale de la vague générée sera fonction de la hauteur d'eau dans le bassin. Les hauteurs de bagues minimales, relatives au niveau d'eau dans le bassin, seront générées lorsque le bassin sera complètement rempli.

Mots-clés : Tsunami généré par un glissement de terrain, glissement partiellement submergé, modélisation numérique, mine à ciel ouvert, glissement rocheux actif.

1. Introduction

Approximately 90 km south of Québec City, on the border between Black Lake sector to the north (part of Thetford Mines) and the municipality of Saint-Joseph-de-Coleraine to the south, is located the open-pit mine *LAC d'Amiante du Canada*, previously operated by the *LAB Chrysotile* company (Fig. 1).The pit-mine was an asbestos mine, which began its operation in 1958, and was completely shutdown in 2012. From a geological point of view, *LAB Chrysotile* installations are located within the Thetford-Mines Ophiolite Complex (Schroetter et al. 2005). The eastern wall of the main pit, i.e. the wall where the studied landslide occurred, is mainly composed of partially serpentinized peridotite. A granitic dyke is also observed in the northernmost portion of the east wall.

Many landslides were identified on the periphery of the open-pit mine since 2009. In 2010, a large rockslide involved the west wall of the main pit (Amoushahi et al. accepted). The rockslide scar, with a width of 700 m can be observed in Figure 1. The east wall was significantly affected by a major event in July 2012. A total volume of 20 million of cubic metres (M m³) of rock underwent a vertical displacement of ~100 m (Caudal et al. 2017). Evidences of this movement, such as deformations and fissures on the Highway 112, were observed as early as in 2009. This rockslide destroyed a 1 km long section of the highway (Figure 1). More details concerning the landslide history on the periphery of the mine as well as on the geology of the site are presented by Caudal (2013) and Caudal et al. (2017).

Tension cracks, some of which have a width of about 1 m, were observed during field investigations. Some of them are traced on Fig. 1. Site investigations have revealed a much larger unstable volume than what was mobilized by the July 2012 event. Furthermore, this unstable volume is still active. Analysis of data acquired from airborne and terrestrial LiDAR surveys also revealed surface movements along the east wall. The analysis of inclinometers installed during a drilling campaign coordinated by the Quebec *Ministère des Transports, de la Mobilité durable et de l'Électrification des transports* (MTMDET) also showed displacements. Using these evidences and assuming that the rockslide is occurring along pre-existing and known discontinuities, the potential failure surface was identified. The main scarp location of this potential rockslide is presented in Figure 1. The mobilized volume could potentially reach a

maximum of 50 M m³, making the Black Lake rockslide one of the largest rockslides in Canada (Turmel et al. 2016). Furthermore, since the end of the mining operations, the water pumping system has been stopped, causing the gradual filling of the pit. According to the restoration plan of the mine and a hydraulic study provided by the MTMDET (Thériault and Boutet 2013) the final elevation of the water surface relative to the mean sea level will be between 232 and 233 m, which is only 2 - 3 m below the regional highway adjacent to the pit, which is at an elevation of 235.6 m. The outlet of the lake will be constructed in the future, and is planned to be constructed to the east of the open pit, as pointed out on Fig. 1. The exact geometry is still unknown, so it cannot be included in the calculations. With such a landslide volume, and considering the limited volume of the open pit mine (approximately 230 M m³ of water when completely filled) as well as the gradual rise of the water level into the open pit, it is then crucial to look at the landslide potential to generate tsunami. This could be done by either of the following methods;

i)   physical modeling, which would replicate on a small scale level the landslide and geometry of the pit (e.g. Lindstrøm et al. 2014),

ii)   using empirical relationships to establish initial wave generation (e.g. Heller et al. 2009),

iii)   or using numerical models to calculate wave propagation (e.g. methodology used by BGC 2012).

In either case, the different scenarios are partially submerged landslides. The different empirical relationships for wave generation found by the authors are for subaerial landslides or for wholly submerged landslides. In addition, scaling effects from physical experiments (see e,g, Pedersen et al. 2013) introduces a bias that needs to be corrected for, which points to application of numerical models. Physical modeling of a scale model of the geometry in question (such as done by Lindstrøm et al. 2014) was not considered here due to the cost involved in such analysis. However, if movements are still present when the open pit will be almost at his capacity, this option may be done in order to have better constrains on the tsunami The solution considered in this analysis was then to consider wave generation and propagation as a whole, and the depth averaged non-linear shallow water (NLSW) model GeoClaw software did permit to simulate both generation and propagation. Granted, the bias related to using a depth averaged model for the present problem, which is intrinsically three-dimensional, is large, and a more comprehensive three-dimensional hydrodynamic treatment (e.g. Gisler et al. 2006; Basu et al. 2009; Biscarini 2010; Abadie et al. 2012) would represent the physics better. Still, given the large uncertainties in question, and because modeling techniques for propagation

and generation using the primitive Navier-Stokes equations are still not as mature as for depth averaged models due to their less accurate free surface representation, we considered the Geoclaw model sufficient for the present investigation.

The tsunami modelling results will be used to identify the minimum water level required in the open pit at which the road and urban infrastructures would be affected by the inundation and estimate the potential impact, in terms of inundation, if a sudden acceleration of the landslide was to occur. Such waves could reach urban and road infrastructures in the vicinity of the mine, that are at elevations between 260 metres and 235.6, i.e. 28-2 m above the final elevation when the lake will be completely filled. If tsunamis were generated, and in the case they reach the road or the urban infrastructures, water would be drained in a small creek located nearby the road. In that case, the next inhabited area would be at more than 7 km of distance, and won't be considered in the analysis.

Selected plausible rockslide scenarios were chosen in order to define the different input parameters of the analysis. These parameters represent the topography and bathymetry of the study area, the water level in the main pit, the landslide volume and geometry and finally the velocities and accelerations developed by the mobilized mass. To determine the wave generation potential, different scenarios are analyzed, using a numerical model to simulate landslide-generated tsunami, to characterize the generation, propagation and inundation processes.

In the past, many cases of rockslides have generated a wave during their mobilization in a water basin such as an open-pit mine, a reservoir, a lake, a fjord or a river worldwide, for instance Lituya Bay 1958 (Miller 1960; Fritz 2002; Fritz et al. 2009), Vaiont Dam 1963 (Kiersch 1964; Müller 1964, 1968, Ghirotti 2012), Yanahuin Lake 1971 (Plafker et al. 1979), Tafjord (Harbitz et al. 1993), and more recently due to the Chehalis Lake 2012 (Wang et al. 2015) and Lake Askja 2014 rockslides (Gylfadottir et al. 2017). The case of Black Lake differs from most of the cases described in the literature since it involves a partially submerged landslide, where the equilibrium water depth will vary depending of the timing of the impact. Often, the literature describes either subaerial landslides, where the foot of the failure surface is located above the water surface, or submarine landslides, where all the mass is completely submerged. However, tsunami generation for a partially submerged landslide was modelled for the hypothetical La Palma case by Løvholt et al. (2008) and Abadie et al. (2012).

In this paper, numerical modeling software used in this particular project, the GeoClaw software, will be described. All the input parameters required for the modeling will be presented and finally, one of the studied scenarios is presented and discussed in details.

2. Methodology

The general approach used in this study to determine the potential rockslide scenarios is divided in three main steps: (1) Stability analysis, (2) landslide dynamics and (3) numerical modelling of the tsunami. This paper will, after presentation of results from stability analysis and landslide dynamics, mostly concentrate on the third aspect, the numerical modelling of the tsunami, the other component of this study are discussed in more details in Turmel et al. (2015) and in a report by Turmel et al. (2016), for which a hyperlink is provided in the reference list.

Slope stability analysis previously carried out by Grenon et al. (2017) and in Turmel et al. (2016) analyses were used to define the volume and geometry of potential landslides. Geotechnics parameters were obtained with a back analysis of the July 2012 rockslide case on the open-pit east wall and by the use of informations provided by the mine. A total of four plausible scenarios were obtained and are named: Global, Big South, Little South and Volume behind July 2012 event scenarios. Only the Global scenario is described in this paper.

The NIS numerical model (Norem et al. 1987) was used to numerically model the mass transport in order to obtain an estimate of the velocity reached during mobilization. The rheology used in this software is a modified version of a CEF fluid (Criminale et al. 1958). The constitutive equation for the shear stress is:

$$\tau_{xy} = c + \sigma(1 - r_u)\tan\phi + m\bar{\rho}\left(\frac{dv}{dy}\right)^r \tag{1}$$

In eq. 1, c represents the cohesion (or the yield strength), σ the total vertical stress at the base, m the viscosity of the material, ρ the mean volumetric mass of the flowing material and r is an exponent equal to 2 (Norem et al. 1990) for a landslide in inertial regime. This exponent would be 1 in a viscous regime. Finally, r_u is the ratio of pore water pressure, defined as:

$$r_u = \frac{u}{\gamma_t H_s}$$

(2)

Where u is the pore-water pressure, γ_t the total unit weight of the soil and H_s the height of the soil column. The first and third term on the right hand side of eq. 1 relates to the viscous aspect of the material where the second term on the right hand side of eq. 1 defines the plasticity of the material as a function of the vertical stress, pore pressure and friction (Locat and Lee 2005). This software was first developed by Norem et al. (1987, 1989) to model snow avalanches, it has subsequently been adapted for submarine landslides by Norem et al. (1991) and for rockslides (Locat et al. 1992; Harbitz and Glimsdal 2014). This diversity of application of NIS is caused by the rheological model used, that incorporates visco-plastic as well as frictional terms. From the July 2012 event back analysis, model parameters were calibrated, such as friction coefficient and shear stress viscosity. A parametric analysis was used to determine two velocity profiles for the Global scenario: slower but more likely velocities (i.e. slow) and quicker but less likely velocities (i.e. rapid). In these analyses, the presence of water is not considered, in the sense that the landslide is simulated as happening in the air and not in the water. As this will lead to higher velocities, the values obtained are conservative.

Finally, a numerical modeling tool, the GeoClaw software (LeVeque 1996; LeVeque 1997; Berger et al. 1998), was used to determine the wave generation potential of the plausible partly-submerged rockslide scenarios. Based on the non-linear shallow water equations (NLSW), the generation, propagation and inundation processes were characterized using mainly synthetic wave gauges strategically located on the lake free surface and on the potentially vulnerable infrastructures.

2.1.   GeoClaw software

The Geoclaw software has been mainly chosen for its simplicity and numerical robustness and for its capacity to resolve shocks and boundary flow problems (i.e. inundation and flooding). Furthermore, the robust numerical approach used here was favourable due to the complex bathymetry, in which more sophisticated non-hydrostatic models often are hampered with instabilities (Løvholt and Pedersen 2009; Løvholt et al. 2013). The numerical methods within ClawPack is described in details by Berger et al. (2011) and by LeVeque (2004). It was designed to

solve hyperbolic systems of partial differential equations in one, two or three dimensions (Berger et al. 2011). More specifically, the GeoClaw model applied here solves the NLSW model using a finite volume technique, allowing for drying and wetting. A bottom friction term is also included in GeoClaw model, defined using a Manning coefficient (LeVeque et al. 2011) of 0.025 for all simulations. GeoClaw also features an Adaptive Mesh Refinement tool (AMR) allowing an increase in the resolution of the grid cells in regions of interest where wave propagation occurs. GeoClaw software has already been tested for rockslide tsunamis in complex fjords (Harbitz et al. 2014), where comparisons were made between GeoClaw and the ComMit/MOST model (NGI, 2010). It was found (NGI, 2010) that both these models produce relatively similar run-up height, and that the MOST model might be more conservative than GeoClaw. MOST model is a standard model and is commonly used worldwide. A dispersive version of the GeoClaw model (Kim et al. 2017) was also used for simulating the Askja rockslide-induced tsunami (Gylfadôttir et al. 2017). They showed that the use of a Boussinesq model did reduce the wave height of the first crest, as compared to the NLSW equations used in GeoClaw. Hence, GeoClaw would often produce more conservative results for the leading wave compared to the Boussinesq model.

The wave is initially generated by the initial geometry deformation of the main pit due to mobilized rockslide, causing a local elevation (in front of the slide) or through (at the back of the slide) of the water depth. The time dependent displacements of this mass are determined from the center of mass for the slide modeled using NIS software. In GeoClaw, the mass will move as a flexible blanket, in the sense that the rockslide is not allowed to elongate, but only to slide. This approach is plausible for the Black Lake case if we consider that the future landslide moves as a translational failure, and where the displacement is minimal, such as it was the case for the 2012 landslide, and where the mass did not dislocate to a great extent. Moreover, initial acceleration often governs the tsunamigenesis in such cases and post deformation pattern is of limited importance (Løvholt et al. 2015).

The generated model is a one-way coupled model, where the scheme is taking into account the account the time dependent change in water depth in the momentum equation (see e.g. Leveque et al. 2011). This modifies both the volumetric flux and adds momentum of the shallow water waves in each time step. However, one-way implies here that the momentum transfer from the slide to the water column is taken into account, but the momentum from the water to the landslide is ignored.

2.2.   Input parameters

Information regarding the study area must be integrated into the GeoClaw software so that it can model the wave generation, propagation and inundation. First, the topography of the study area must be known, as well as the elevation of the initial water level in the pit. Secondly, we need to define the landslide volume and geometry as well as its velocity profile over time following a sudden acceleration.

For this particular project, many different rockslide scenarios were studied (Leblanc 2016; Turmel et al. 2015), but in this paper, only the results associated with the scenario that addresses the entire mass as a whole is presented.

2.2.1.   Topography and bathymetry of the site

Topographic and bathymetric data were obtained from airborne LiDAR surveys conducted between 2010 and 2014. The bottom topography of the main pit is only visible on the 2010 survey. The bottom topography is hidden in subsequent surveys since LiDAR cannot acquire underwater data. To obtain a digital elevation model including the deformations observed on the edge of the mine since 2012 as well as the bottom topography, the 2014 airborne LiDAR survey was merged with the 2010 survey. The final digital elevation model used for the modeling, with a regular grid of 5 m x 5 m, is shown in Fig 2.

2.2.2.   Open pit flooding process

The end of mining operations caused the complete shutdown of the pumping system whose goal was to prevent the rise of water level in the pit. According to the mine restauration plans and the MTMDET hydraulic study of the site, the final water level should reach an elevation of 233 m above sea level. The 2014 airborne LiDAR survey revealed that the water level has reached an elevation of about 75 m above sea level (asl). The minimum elevation of the pit is approximately 45 m below sea level (bsl). The average filling rate of the main pit was calculated and it was estimated that the water elevation in the mine will reach its final elevation in 2035. Figure 2 shows contour lines associated with the water elevation for which the wave modeling was done.

2.2.3. Water gauges location

Synthetic wave gauges were used to provide time series of water surface elevation or on-land flow depth. They also enable to observe the time of arrival of the wave at the fixed point and the duration of the disturbance. At time $t = 0$, the water gauge floats on the free surface and the recorded elevation is equivalent to that of the free surface. In the case where the water gauge is located on dry land, its initial elevation is equal to its elevation relative to the initial water surface, and thus do not represent the elevation of the water surface until water reach the water gauge. This condition allows observing the flow depth during the inundation process. Figure 1 presents the locations of the water gauges used in the analysis. The water gauge 01 is located on the lake free surface, regardless of the initial water elevation. It allows determining the maximal free surface elevation during the wave propagation. Two water gauges are located on the new Highway 112 to characterize the potential inundation of the infrastructure. The water gauge 04 is located north of the lake at a point where the difference between the road elevation and the free surface is minimal (elevation of 235.6 m asl). The water gauge 06 is further south of the study area, near the future lake shoreline, with an elevation of about 257 m asl. Finally, three water gauges are located northeast of the study area and are associated with the City of Thetford Mines (water gauges 02, 03 and 08). Each is located at a significantly different elevation, characterizing three main areas potentially vulnerable to inundation (251.10 m, 247.1 m and 235.9 m for the water gauges 02, 03 and 08 respectively).

2.2.4. Landslide volume and geometry scenarios

As previously mentioned, following the July 2012 event, a large volume of unstable rocks is still present with signs of movements. Despite the impossibility to acquire data related to the depth of the failure surface or structural measurements, due to site inaccessibility, the probable geometry of the global rockslide was evaluated. From the analysis of terrestrial LiDAR surveys and using Coltop software, Caudal et al. (2014a and 2014b) presents a stereonet of the identified joints regrouped in three (3) discontinuity families that characterized the rockslide. These discontinuity families are considered similar to the information provided by the mining company LAB Chrysotile concerning three main discontinuity families in the mine east wall. The plausible rupture surface was defined

assuming that the landslide partially occurs along some of these pre-existing discontinuities rather than inside the intact rock mass. Should this be the real failure surface, the maximum potential volume would be around 50 M m³. The first volume and geometry scenario used as input parameters for the numerical modeling, named Global scenario, represents the whole volume (Fig. 2). For this project, some other landslide geometries were also analysed, and the results are reported in Turmel et al. (2016). However, since the results are not reported here, details on these scenarios won't be elaborated. It was decided to report only results from the global scenario since this scenario shows the largest waves, and is the most critical in terms of wave generation.

A stability analysis was done by Turmel et al. (2016) on the Global potential rockslide scenario, on the profile shown in fig. 1. The geological and geotechnical model used in this analysis (Fig. 3) was deducted based on mining company information, and no boring was made for this particular project in order to confirm this geological model. The results show that with geotechnical parameters reported in table 1 which are average values derived from rock mass characteristics provided by several modelling, laboratory testing and field measurement sources (see Grenon et al. 2017 for all the details) and with cohesionless material (assumption reasonable given the actual large displacement of the failed mass), the factor of safety would be about unity when the water level is at an elevation of 45 m below sea level, i.e. when the pumping of the water by the mine was still active and the open pit was free of water. This is the expected result since the landslide activity was visible before the mine flooding. Thereafter, a prospective analysis of the evolution of the factor of safety with the water level elevation in the main pit was conducted for two different scenarios of groundwater table position in the slope (Fig. 3 and 4), one with a higher groundwater level and one with a lower groundwater level. The exact location of the groundwater table is unknown. The scenario of the most critical groundwater table, which is also the scenario illustrated in Fig. 3 (the darker line), shows that the minimum factor of safety would be reached when the water level is at 0 m (this is purely coincidental that the lower factor of safety happens at an elevation of 0 m), before increasing with higher water level. This factor of safety is less than unity until the water level reaches an elevation of about 100 m. This is in accordance with back-analysis of the 2012 landslide made by Caudal et al. (2017) where he found similar results for the 2012 landslide, and where, in the 2012 portion of the landslide, the water table level is approximately the same as in the worst case presented here. However, it is important to mention that the factor of safety remains close to the stability limit (about 1.2) even when the lake level

reaches its final elevation of 233 m. Many uncertainties remain connected with this prospective analysis, notably the real position of the failure surface and of the groundwater table, the nature and the geotechnical properties of the rock and debris involved and the groundwater flow in the rock mass.

2.2.5. Scenarios with different landslide dynamics

NIS software (Norem et al. 1987) was used to numerically model a mass propagation in order to obtain an estimation of the velocities during its mobilization. Its operation is described in detail in the works of Turmel et al. (2015, 2016).

The July 2012 event was used to determine the values of the parameters in the model. Unfortunately, nobody was present when the landslide did happen, and no measurements of velocity were available. Back-analysis was then possible only by calibrating the post-failure topography obtained by the numerical analysis with the post-failure obtained from LiDAR survey. For the Black Lake case, it is believed that the movement is mostly controlled by the frictional term, since the whole volume did move in one block and was not disintegrated such as what was seen, by example, in Bingham Canyon (e.g. Moore et al. 2017).Two parameters must then be defined in the model, the friction angle φ and the shear stress viscosity m. In the back analysis, the material mean density remained constant at 3200 kg/m³ (assumed representative of the observed peridotite on site). The two parameters, the friction angle and the shear stress viscosity, were varied in order to reproduce the July 2012 rockslide morphology taken from its mobilization at the bottom of the main pit. As the exact position of the water table was unknown at the time of failure, it was considered, as simplification, that the r_u term, in eq. 1, was 0 in this back-analysis, meaning that the surface of rupture was considered as dry, which may not been has the case. Using this hypothesis, a friction angle of 33.5° was found to reproduce the best the morphology of the 2012 landslide. According to Hungr and Morgenstern (1984), dynamic friction angle should be 2 to 4 degrees less than the static friction angle. The 33.5° found can then be considered as plausible for the 2012 landslide. The shear stress viscosity used in the back-analysis was kept very low and did not influence the behaviour of the landslide.

The parameters derived from the July 2012 event back analysis above were used to determine the velocity evolution of all potential rockslide scenarios evaluated. In the case of the Global scenario, the presence of water on

the rupture surface was also taken into account, by modifying the r_u parameter in eq. 1. This has as effect to decrease the apparent or effective friction angle values. A decrease in the friction coefficient might also be justified by the uncertainty on the exact angle of the failure surface and the exact nature of the materials. Two different values of r_u were used in eq. 1, i.e. a value of 0.17 and a value of 0.30, which correspond to apparent or effective friction angle values of 25° and 29° respectively. Using eq. 2, one could demonstrate that, with a mean density of the material of 3200 kg/m³, a r_u value of 0.17 correspond to a mean water height which is 55 % of the total height of the soil over the surface of rupture. A r_u value of 0.3 correspond to a mean water height which is 95% of the total height of the soil over the surface of rupture, i.e. the phreatic surface being almost at the ground surface. The use of the friction angle of 33.5°, i.e. with a r_u of 0, would only cause displacements of 8 m with relatively low velocities. For the two other scenarios, similar morphology is observed after the mass mobilization, but as expected, the lower friction angle generates the largest spreading distance of the debris. Figure 5a shows the final morphology of the mass along the A-A' section (Fig. 1) for an apparent friction angle of 25° and 29°. It is also possible to observe on Fig. 5a the pre-failure topography as well as the simplified modeled topography used for the simulation and the sliding surface modeled.

As mentioned previously, the velocity scenarios do not take into account the presence of water in the open pit, only on the failure surface. For a partially or entirely submerged landslide, two forces are acting against the movement, i.e. a drag force and the added mass force. The added mass force is a function of the acceleration of the landslide, where the drag force is a function of the speed of the landslide. The initial acceleration as well as the velocity reached by the landslide, if underwater, would be lower than in air, so lower than the profiles calculated with NIS. The scenario proposed here with the lowest apparent friction angle could then be considered as an extreme case, since it considers that the phreatic surface is almost at the ground surface, meaning the lowest possible friction, and that it do not consider added mass force nor drag force, that would act to restrain the movement.

Figure 5b presents the profile of the rockslide center of mass velocity against its travel distance during its mobilization. For both scenarios identified above in the Global rockslide analysis, the velocity profiles are similar, with a rapid initial acceleration during the first ten metres followed by a plateau where the velocity is approximately constant and finally a rapid deceleration. The initial acceleration (*a*) for both scenarios is about 1.6 m/s², which is in

the same range as acceleration of other described landslides in the literature such as Bingham canyon landslide (a = 2.1 m/s², Hibert et al. 2014) or Mount Meager (a = 0.4 m/s², Allstadt, 2013). The maximal velocity is respectively of 10 and 6 m/s for the effective friction angle scenarios of 25° and 29° respectively. These velocities are relatively low compared to the presented cases in the literature (e.g. Bingham Canyon: 37 m/s (Hibert et al. 2014), Mount Meager: 15 m/s (Allstadt 2013); Pandemonium Creek: 80 - 100 m/s (Evans et al. 1989)) and are explained by the short distance between the rockslide tip and the slope foot, causing a short acceleration distance before deceleration.

3. Numerical modelling results

Tsunami wave generation from the rockslides were modeled using multiple combinations of lake level and velocity profiles. Two cases will be illustrated next, one with a lower lake level and one with a higher lake level.

Figure 6 illustrates the numerical modeling results for selected time steps for the global landslide, using slow velocity scenarios and an initial lake level of 150 m asl. The lake level was selected from the factor of safety sensitivity analysis and corresponds to a lake level slightly exceeding the identified critical range (i.e. factor of safety less than unity). From the lake at rest (Fig. 6a), a wave front, 17 m high, is first formed by the mass mobilization (Fig. 6b). This wave reaches an elevation of about 167 m asl. This wave propagates (Fig. 6c) to the other side of the basin, and negative amplitudes are seen behind the landslide. In this scenario, the initial lake level is too low for the wave to inundate farther than the open pit, and the water surface will eventually come to rest (Fig. 6d). The water level is initially low enough to prevent inundation of any major infrastructures in the vicinity of the mine. The volume of the rockslide is such that the water level is increased by about 3 m 10 minutes after the mass mobilization.

The wave propagation numerical modeling results for gauge 4, located over the road, for the scenarios with friction angle of 25° (rapid scenario) and 29° degree (slow scenario) when the lake will be completely full (233 m asl) are graphically presented in Figure 7. The 0 value on the vertical axis represent the road elevation. Approximately 1 minute after the landslide, the wave will reach the road. For the rapid velocity scenario, the tsunami height will be approximately 12 m high, and for the slower scenario, the tsunami height will be about 3.5 m. This wave has a short duration, after 1.5 minutes, the water level will have decreased to about 2 m and 1 m for the rapid and slow scenario

respectively. Reflection in the basin will generate other waves, as shown on the hydrograph. It has to be noted here that the elevation after 6 minutes should decrease for the rapid scenario, but the water was not allowed to leave the numerical domain, so it cannot fully drain. The effect of a faster landslide is clearly seen here, where waves from the faster scenario are always higher, and the first arrival is faster. However, the shape of both curves is approximately the same.

Figure 8 presents the maximum surface elevation reached by the wave at the water gauge 01 for different scenarios of the initial lake surface elevation. Results are presented for gauge 01 here because results from this gauge are not affected by abrupt changes in topography. The box in Figure 8 identifies the water level range where a sudden acceleration of the mass is most probable, thus where the factor of safety is less than unity. The horizontal dashed line illustrates the inundation threshold corresponding to the minimum surface elevation that the generated wave has to reach at water gauge 01 to inundate Highway 112 at gauge 04. This inundation threshold for the slower scenario (Fig. 8a) is 231 m and would occur for a lake level of 225 m asl (Fig. 8a). At this level of 225 m, the first traces of inundation (some centimeters) would be observed on water gauge 04, corresponding to the most vulnerable portion of Highway 112. Hence, in that case, if the water level in the main pit where gauge 01 is located reaches 231.4 m, the topography will lead to an inundation of the road, which is located at an elevation of 233.6 m asl. This effect of topography is illustrated in Fig 9, where the wave gauge for both gauge 01 and 04 are shown, for an initial lake elevation of 226 m asl, this elevation was chosen since at 225 m, the wave was only a few centimeters high and not clearly visible on such figures. At that lake elevation, the maximum free surface elevation reached inside the basin is slightly over 232 m, where the road, at 233.6 m, will be submerged by a 25 cm high wave.

Still for the slow velocity scenario, the highway would also be affected in the southwest portion, at water gauge 06, when the lake level is at 233 m asl (i.e. when the pit is full), with a flow depth of 0.3 m. Furthermore, at this lake level (233 m), the City of Thetford Mines would be affected, at water gauge 08, where the flow depth would be 1 m. In Thetford Mines, only this water gauge would be affected by inundation: water would never reach water gauges 02 and 03, even if the lake level reaches 235 m. It is important to note here that in the critical area defined by a factor of safety less than unity (boxed in Fig. 8), the numerical modeling results demonstrate that no inundation would reach the potentially vulnerable infrastructures.

The numerical modeling results concerning the rapid velocities scenario (scenario where the friction angle is 25°) are also graphically presented in Figure 8b, showing the maximum surface elevations reached by the wave at water gauge 01 for different initial water level scenarios in the lake. The same critical area, defined by the water level range where a sudden acceleration of the mass is the most likely, is delimited by a box. Compared with the slow velocities scenario (ϕ = 29°), it is possible to notice that greater surface elevations are observed. Indeed, the minimum water level at which the inundation of a first infrastructure is observed would be 195 m (Fig. 8b). The inundation threshold would corresponds to a surface elevation of 215 m at water gauge 01 and the first traces of inundation would be observed on the portion of highway 112 observed at water gauge 04. When the initial lake level reaches 215 m elevation asl, the southwest portion of highway 112 (water gauge 06) would be affected by a flow depth of 0.3 m. The City of Thetford Mines would be affected when the lake level reached 215 m, where the first traces of inundation are observed at water gauge 08. A flow depth of 1 m is measured at water gauge 03 when the water level reached 230 m. Water gauge 02, on the other hand, would never be affected by inundation, even when the lake level reaches 235 m. However, as in the case of the slow velocity scenario previously described, the identified critical water levels are associated with factor of safety greater than unity. In the critical range, when the water level is between 0 m and 120 m asl (i.e. factor of safety less than unity), no inundation is observed, neither on the Highway 112 (water gauges 04 and 06) nor in Thetford Mines (water gauges 02, 03 and 08). The results of numerical modeling showing a potential to reach one of the infrastructures, for both slow velocity scenarios (ϕ = 29°) and rapid velocity scenarios (ϕ = 25°), are presented in Table 2.

4. Analysis of numerical modelling results

By comparing the maximum elevation reached by the generated wave relative to the initial water surface elevation, it is possible to observe that lower water depths leads to higher wave amplitudes (relative to the lake level). For example, results from Global scenario show a maximum water height of 15.3 m (for the rapid velocity scenario) and 6 m (for slow velocity scenario) at water gauge 01 in the pit relative to the initial water surface at an elevation of 233 m (Table 2). At 150 m, at the same water gauge location, the maximum wave height is of 28 m (for rapid velocity scenario) and 17 m (for slow velocity scenario). This tendency is explained by the subaerial component of the Global

rockslide. This component is more important when the water level is lower (i.e. the partially submerged rockslide has a greater subaerial portion). The wave height is proportional to the ratio between subaerial and submerged portion of the rockslide as more energy is transferred to the water basin (Fine et al. 2003). Furthermore, since the open pit volume is small, the displacement of the landslide will increase the equilibrium height after landslide event. For an elevation of 150 m, this increase will be of about 3 m for the slow velocity scenario and of about 12 m for the rapid velocity scenario (rapid velocity scenario has greater displacements, hence a greater submerged portion of the mass) while for an elevation of 233 m, this increase will be lower, i.e. 2 m (Fig. 9). However, being a partially submerged landslide and not a totally submerged landslide, it is believed that the behaviour of this translational landslide will behave more and more like a submerged landslide when the lake still water level increases with time. For fully submerged slides, the wave generation is different from subaerial slide, and also controlled by the landslide acceleration in addition to the slide speed (Løvholt et al. 2015).

However, for Black Lake case, higher generated wave does not necessarily mean greater flooding, mainly because of the pit geometry. The elevation of Highway 112 relative to the water surface elevation is of 2.6 m when the water surface is at 233 m and is of 85.6 m when the water surface is at 150 m. The relative elevation difference is increasing rapidly with the water level diminution because of the pit wall that the wave must cross before being able to flood Highway 112. The generated wave is thus trapped in the pit when the water level is too low (i.e. lower than the identified critical water level).

Numerical modeling results revealed higher generated waves for the fastest velocity scenario. However, rapid and slow velocity scenarios are not only different in terms of velocity, but also in terms of center of mass traveled distance (Fig. 5b). The traveled distance is of about 200 m for the rapid scenario while it is of about 75 m for the slow scenario.

The results demonstrate the generation of a single wave front as from a piston pushing the water column. Reflections in the basin will then happen. Moreover, wave amplitude and wavelength are largely greater than water depth, confirming compliance with the most important applicability criterion of the model. However, if landslides are still active when the water level reaches the most critical levels where inundations would be possible, more advanced numerical models, such as full 3D Navier Stokes modeling without any simplification, should be used to refine the results. Moreover, wave propagation distances are very short due to the study area topography: numerical modeling

results show that the wave front floods the lake shoreline as soon as the wave generation is finished. The NLSW model does not take into account the dispersive nature of a propagating wave in a water pond. Gylfadottir et al. (2017) have demonstrated that dispersion is likely to occur with a subaerial impact tsunami. Usage of dispersive numerical model (Boussinesq type model for example) gives a different wave radiation pattern compared to a NLSW model. This could result in artificial offsets in run-up calculation. When dispersion is not taken into account, the generated leading wave tends to have a much higher amplitude than when dispersion acts to spread out the wave energy (Gylfadottir et al. 2017), meaning that in this prospective analysis, the maximum wave height found may be higher than what would be calculated using a dispersive scheme, i.e. calculations are on the conservative side. However, as mentioned previously, in the case that landslides are still active when the water level in the lake will reach critical levels, more refined numerical modeling using full-3D Navier Stokes equations or physical modeling using scaled models of the landslide should be done. Some of these more sophisticated models include Flow-3D which has already been used to reproduce physical model experiments (Basu and al. 2009), OpenFOAM which was used to model landslide on river banks that generated tsunami (Locat et al. 2017), Fluent (Biscarini 2010) that was used to simulate the 1958 Lituya bay tsunami in a 2D simplified geometry or Smoothed particle hydrodynamics (SPH) codes that were also used to replicate laboratory experiments (e.g. Yeylaghi et al. 2017). Furthermore, a more complete geotechnical analysis, including boreholes that will reach the sliding surface, will have to be done in order to refine the geological model, since the slope stability analysis done show that the factor of safety for the slope should show an increase, i.e. the slope should become more stable.

5. Conclusions

The main objective of the project was to develop a parameter sensitivity analysis for assessing the hazards of the potentially exposed Black Lake sector of the City of Thetford Mines related to the tsunamigenic potential that could be generated by a landslide impacting the LAB Chrysotile open-pit mine. To meet this objective, the rockslide morphology was determined. Thereafter, kinematic analysis was performed for each of the potential rockslides to

characterize the mass mobilization. Finally, the wave generation potential for each scenario was studied using a numerical modeling tool with different water level in the pit. In this paper, mostly the wave generation and propagation portion of the project was presented in details.

A prospective analysis of the Global scenario slope stability was performed by varying water level in the open pit. Factor of safety evolution according to water level shows a decrease of the factor of safety (FOS) due to a water level increase, followed by a minimum FOS before a constant FOS increase. The minimal FOS was reached when the water level was at an elevation of 0 m in the pit before increasing gradually. FOS of 1 should be reached when the water level is of 100 m. At the final anticipated water level (i.e. 233 m), FOS should be slightly greater than unity, precisely at about 1.2.

GeoClaw software has been used to perform the numerical modeling of the potentially generated tsunami of the Global scenario. For each established velocity scenario, simulations were carried out at several water levels. The critical water level, at which flooding of at least one infrastructure is observed, has been identified. With the strategically located water gauges in the study area, areas where flooding could take place were identified with their corresponding flow depth. For all the velocity profiles used, it was noted that, when the factor of safety of the global slope is under unity, no waves could affect the different infrastructures in the vicinity of the open pit. However, this was possible when the water level in the pit is higher, but in these cases, the factor of safety would be above unity and the likelihood of a global landslide is reduced. Results from the simulations also clearly illustrate the effect of the water level into the pit on the wave height. Relative to the water level, the highest wave height will be when the lake level is lowest, where the lowest wave height will be when the lake level is at its highest level.

Finally, this study provides an example of a prospective approach to study tsunami generation potential in an abandoned open pit mine where landslides can take place. As discussed, if the landslide are still active some years before the lake level will be near critical heights, a more complete geotechnical characterization of the landslide will have to be undertaken to better constrain the velocity scenarios, and more advanced numerical simulations, using for instance full 3D Navier-Stokes models, or physical simulations, will have to be undertaken in order to refine results from this study.

6. Acknowledgments

7. References

Abadie, S.M., Harris, J.C., Grilli, S.T., and Fabre, R. 2012. Numerical modeling of tsunami waves generated by the flank collapse of the Cumbre Vieja Volcano (La Palma, Canary Islands): Tsunami source and near field effects. Journal of Geophysical Research, **117**(C5), 26 pp.

Allstadt, K. 2013. Extracting source characteristics and dynamics of the August 2010 Mount Meager landslide from broadband seismograms. Journal of geophysical research, **118**: 1472-1490.

Amoushahi, S., Grenon, M., Locat, J., and Turmel, D. accepted. Deterministic and probabilistic stability analysis of a mining rock slope in the vicinity of a major public road – case study of the LAB Chrysotile mine in Canada. submitted to Canadian Geotechnical Journal.

Basu, D., Green, S., Das, K., Janetzke, R. and Stamatakos, J. 2009. Navier-Stokes simulations of surface waves generated by submarine landslides: effects of slide geometry and turbulence. 2009 Society of Petroleum Engineers Americas Environmental & Safety Conference, Santo Antonio, Texas.

Berger, M. J., George, D. L., LeVeque, R. J., and Mandli, K. T. 2011. The GeoClaw software for depth-averaged flows with adaptive refinement. Advances in Water Resources, **34**: 1195-1206.

Berger, M. J., and LeVeque, R. J. 1998. Adaptive mesh refinement using Wave-Propagation Algorithms for Hyperbolic Systems. SIAM Journal of Numerical Analysis, **35**: 2298-2316.

BGC Engineering, 2012. Mitchell pit landslide generated wave modelling, Appendix 4-E; BGC Engineering Inc. report, Vancouver, BC. Canada

Biscarini, C. 2010. Computational fluid dynamics modelling of landslide generated water waves. Landslides, **7**(2): 117-124.

Caudal, P. 2013. Analyse d'un glissement actif par suivi LiDAR et modélisation de la rupture: Mine LAB Chrysotile à Black Lake (Québec). Conservatoire National des Arts et Métiers, Paris, France.

Caudal, P., Grenon, M., Locat, J., and Turmel, D. 2014a. Caractérisation et surveillance d'un glissement rocheux actif d'une mine à ciel ouvert en utilisant le LiDAR. Proceedings of Geohazards 6, 15-18 juin 2014, Kingston, Canada.

Caudal, P., Grenon, M., and Fabre, D. 2014b. Suivi LiDAR et analyse de la stabilité d'un glissement de versant à la mine LAB Chrysotile, Black Lake, Québec, Canada. Proceedings of RSS 2014, 2-4 avril 2014, Marrakesch, Morocco.

Caudal, P., Grenon, M., Turmel, D., and Locat, J. 2017. Analysis of large rock failure on the East wall of the LAB mine in Canada – LiDAR monitoring and displacement analysis. Rock Mechanics and Rock Engineering, **50**(4): 807-824.

Criminale, W. O., Ericksen, J. L., and Fibley, G. L. 1957. Steady shear flow of non-Newtonian fluids. Archive for rational mechanics and analysis, **1(**1): 410-417.

Evans, S.G., Clague, J.J., Woodsworth, G.J., and Hungr, O., 1989, The Pandemonium Creek rock avalanche, British Columbia. Canadian Geotechnical Journal, **26**: 427-446.

Fine, I. V., Rabinovitch, A. B., Thomson, R. E., and Kulikov, E. A. 2003. Numerical modeling of tsunami generation by submarine and subaerial landslides. Submarine Landslides and Tsunamis, Kluwer Academic Publishers, Netherlands: 69-88.

Fritz, H. 2002. Initial phase of landslide generated impulse waves. Swiss Federal Institute of Technology Zürich (ETH Zürich), **14871**: 1-337.

Fritz, H. M., Mohammed, F., and Yoo, J. 2009. Lituya Bay landslide generated mega-tsunami 50th anniversary. Pure and Applied Geophysics, **166**: 153-175.

Grenon, M., Caudal, P., Amoushahi, S., Turmel, D., and Locat, J. 2017. Analysis of a large rock slope failure on the east wall of the LAB Chrysotile mine in Canada: Back analysis, impact of water infilling and miming activity. Rock Mechanics and Rock Engineering, **50**(2): 403-418.

Ghirotti, M. 2012. The 1963 Vaiont landslide, Italy, Landslides: Types, Mechanisms and Modeling. Cambridge University Press, Chapter 29: 359-372.

Gisler, G., Weaver, R., and Gittings, M. 2006. SAGE calculations of the tsunami threat from La Palma, Sci. Tsunami Hazards, **24**, 288– 301.

Gylfadóttir S. S., Kim, J., Helgason, J. K., Brynjolfsson, S., Hoskuldsson, A., Johannesson, T., Harbitz, C. B., and Lovholt, F. 2017. The 2014 Lake Askja rockslide-induced tsunami: optimization of numerical tsunami model using observed data. Journal of Geophysical Research: Oceans, **122**(5): 4110-4122.

Harbitz, C. B., Pedersen, G., and Gjevik, B. 1993. Numerical simulations of large water waves due to landslides. Journal of Hydraulogical Engineering, **119**: 1325-1342.

Harbitz, C.B., Glimsdal, S. Løvholt, F., Kveldsvik, V., Pedersen, G.K., and Jensen, A., 2014. Rockslide tsunamis in complex fjords: From an unstable rock slope at Åkerneset to tsunami risk in western Norway. Coastal Engineering, **88**: 101-122

Harbitz, C. B., and Glimsdal, S. 2014. Evaluation of the flow characteristics of the potential Åkerneset rockslide, western Norway – contributions to the design of laboratory experiments on wave generation. Norwegain Geotechnical Institute report 20061333-01-R.

Heller, V., Hager, W.H., and Minor, H.-E. 2009. Landslide generated impulse waves in reservoirs – Basics and computation. VAW Mitteilung 2011, Boes, R. ed. ETH Zurich, Zurich.

Hibert, C, Ekström, G., and Stark, C.P. 2014. Dynamics of the Bingham Canyon mine landslides from seismic signal analysis. Geophysical research letters, **41:** 4535-4541.

Hungr, O., and Morgenstern, N.R. 1984. Experiments on the flow behaviour of granular materials at high velocity in an open channel. Géotechnique, **34**:3, 405-413.Kiersch, G.A., 1964. Vaiont reservoir disaster. Civil Engineering **34**:2 32-39.

Kim, J., Pedersen, G.K., Lovholt, F., and LeVeque, R.J., 2017. A Boussinesq type extension of the GeoClaw mode – a study of wave breaking phenomena applying dispersive long wave models, Costal Engineering, 122: 75-86

Leblanc, J. 2016. Analyse du potential tsunamigénique des glissements de terrain possibles dans une ancienne mine à ciel ouvert à Black Lake, Québec. Master thesis, Department of Geology and Geological Engineering, Université Laval, Québec, 163 pp.

LeVeque, R. J. 1996. High-resolution conservative algorithms for advection in incompressible flow. SIAM Journal of Numerical Analysis, **33**: 627-665.

LeVeque, R. J. 1997. Wave propagation algorithms for multidimensional hyperbolic systems. Journal of Computational Physics. **131**: 327-353.

LeVeque, R. J. 2004. Finite Volume Methods for Hyperbolic Problems. Cambridge University Press, Cambridge, Royaume Uni.

LeVeque, R.J., George, D.L., and Berger, M.J. 2011. Tsunami modelling with adaptively refined finite volume methods, Acta Numerica, **20**: 211-289

Lindstrøm, E.K., Pedersen, G.K., Jensen, A., Glimsdal, S. 2014. Experiments on slide generated waves in a 1:500 scale fjord model, Coastal Eng., 92, 12-23, ISSN 0378-3839, https://doi.org/10.1016/j.coastaleng.2014.06.010.

Locat, J., Norem H., and Therrien, P. 1992. An approach to rock avalanche dynamics. Proceedings of the 1990 annual meeting of Geological Association of Canada.

Locat, J., and Lee, H. 2005. Subaqueous debris flows. In Jacob, M. & Hungr, O. (Eds.), Debris flow hazards and related phenomena. Springer and Praxis, 203-245.

Locat, J., Turmel, D., Locat, P., Therrien, J., and Létourneau, M. 2017. The 1908 disaster of Notre-Dame-de-la-Salette, Québec, Canada: Analysis of the landslide and tsunami. V. Thakur et al. (eds), Landslides in Sensitive clays, Advance in Natural and Technological Hazards Research 46, Springer, pp. 361-371.

Løvholt, F., Pedersen, G., and Gisler, G. 2008. Oceanic propagation of a potential tsunami from the La Palma Island. Journal of Geophysical Research, **113,** C09026, doi:10.1029/2007JC004603.

Løvholt, F., and Pedersen, G. 2009. Instabilities of Boussinesq models in non-uniform depth. International Journal for numerical methods in fluids, **61**(6): 606 - 637.

Løvholt, F., Lynett, P., and Pedersen, G. 2013. Simulating run-up on steep slopes with operational Boussinesq models; capabilities, spurious effects and instabilities. Nonlinear Processes in Geophysics, **20**: 379-395.

Løvholt, F., Pedersen, G., Harbtiz, C. B., Glimsdal, S. and Kim J. 2015. On the characteristics of landslide tsunamis. Philosophical transactions of the royal society A, **373**(2053): 1-18.

Miller, D. J. 1960. The Alaska earthquake of July 10, 1958: Giant wave in Lituya Bay. Bulletin of the Seismological Society of America, **50:**2 253-266.

Moore, J.R., Pankow, K.L., Ford, S.R., Koper, K.D., Hale, J.M., Aaron, J., and Larsen, C.F. 2017. Dynamics of the Bingham Canyon rock avalanches (Utah, USA) resolved from topographic, seismic and infrasound data. Journal of Geophysical Research: Earth Surface, **122**: 615-640

Müller, L. 1964. The rock slide in the Vaiont Valley. Rock Mechanics and Engineering Geology **2**(3-4): 148–212.

Müller, L. 1968. New considerations on the Vaiont slide. Rock Mechanics and Engineering Geology **6**(1-2): 1–91.

NGI. 2010. The Aknes/Tafjord project – numerical simulations of tsunamis from potential and historical rock slides in Storfjorden; hazard zoning and comparison with 3D laboratory experiments. Norwegian Geotechnical Institute Report 20051018-00-1-R Rev. 01.

Norem, H., Irgens, F., and Schieldrop, B. A. 1987. A continuum model for calculating snow avalanches. In: Avalanche Formation. Movement and Effects, (Salm, B. and Gubler, H., eds.), IAHS Publ. No. 126, 363-379.

Norem H., Irgens F., and Schieldrop, B. 1989. Simulation of snow avalanche flow in run-out zones. Annals of Glaciology 13, 218–225.

Norem, H., Locat, J., and Schieldrop, B. 1991. An approach to the physics and the modeling of submarine flowslides. Marine Georesources & Geotechnology, 1**9**(2): 93-111.

Pedersen, G. K., Lindstrøm, E., Bertelsen, A.F., Jensen, A., Laskovski, D., and Sælevik, G. 2013. Runup and boundary layers on sloping beaches, Physics of Fluids 25:1

Plafker, G., and Eyzaguirre, V.R. 1979. Rock avalanche and wave at Chungar, Peru: Rockslides and avalanches, 2, engineering sites. Elsevier Scientific publishing company, Chapter 7: 269-278.

Schroetter, J.-M., Bédard, J. H., and Tremblay, A. 2005. Structural evolution of the Thetford Mines Ophiolite Complex, Canada: Implications for the southern Québec ophiolitic belt. Tectonics, **24**(TC1001): 1-20.

Thériault, M., and Boutet, J-F. 2013. Étude hydraulique : Canal de sortie et de crue en amont du pont projeté de la route 112. Rapport géotechnique, Roche SNC-Lavalin, 37 pp.

Turmel, D. Leblanc, J., Locat, J., and Grenon, M. 2015. Établissement de scénarios d'accélération et de vitesse de grands glissements rocheux actifs: le cas de Black Lake. *GéoQuébec 2015*.

Turmel, D., Leblanc, J., Locat, J., Locat, A., and Grenon, M. 2016. Projet Black Lake : Évaluation de l'accélération potentielle du glissement de Black Lake et scénarios de tsunami. Rapport final présenté au Ministère des Transports du Québec, décembre 2015, Report LERN-Black-Lake-2015-01 (http://www.bv.transports.gouv.qc.ca/mono/1183051.pdf).

Wang, K., Ward, S.N., and Xiao, L. 2015. Numerical simulation of the December 4, 2007 landslide-generated tsunami in Chehalis Lake, Canada. Geophysical Journal International, **201**(1): 372–376.

Yeylaghi, S., Moab, B., Buckhama, B., Oshkaia, P., Vasquez, J., and Crawford, C. 2017. ISPH modelling of landslide generated waves for rigid and deformable slides in Newtonian and Non-Newtonian reservoir fluids. Advances in Water Resources. June 2017.

Figure Captions

Fig. 1. Hillshade image derived from the DEM of the study area showing the main scarp location of the different mass movement episodes that occurred since 2010 on the perimeter of the abandoned open-pit mine located south of Black Lake. Location of the different numeric water gauges are also marked on the figure. In the inset is the location of the area, marked by a star.

Fig. 2. Geometry of the Global rockslide scenario of 50 M m³. Three contour lines were added for elevations 150, 200 and 233 m.

Fig. 3. Geological and geotechnical model used for the slope stability analysis. In this case, the water level is of 100 m.

Fig. 4. Factor of safety evolution of the Global rockslide as a function of pit flooding for two different water table scenarios in the rock mass, illustrated on Fig. 2.

Fig. 5. a) Used profiles for the Global rockslide NIS modelling with the spreading results from two different friction angles. The cross-section used for the 2D topographic profiles is shown in Fig. 1. b) Velocity evolution with center of mass traveled distance for the two velocity scenarios of the Global rockslide.

Fig. 6 : Plan view of the numerical modeling results of the global landslide, using rapid velocity scenario and an initial lake water level of 150 m. North is up.

Fig. 7. Water height above road (gauge 04) for the two velocity scenarios when the lake will be at its maximum water level (233 m) capacity (Global landslide).

Fig. 8. Maximal elevation reached by the wave in the main pit at water gauge 01 (Fig. 1) for different initial free surface elevation for the Global scenario and with the slow velocity profile in (a) and rapid velocity profile in (b). The red box delimits the zone where the factor of safety is lower than unity.

Fig. 9. Results from the simulations with the slow velocity scenario, for gauges 01 and 04, when the lake will be filled up to an elevation of 226 m (Global landslide).

Table 1 Geotechnical properties used in the back-analysis

Lithology	Unit weight (kN/m^3)	Friction angle (°)
Massive serpentinite	25	30
Semi-schistose serpentinite	25	23
Schistose serpentinite	25	19
Massive peridotite	27.5	37
Fractured peridotite	27.5	35
2012 landslide debris	20	30
Tailings	22	30

Table 2 Numerical modelling results of the Global rockslide generating a wave that can reach the infrastructures.

		Surface elevation (m)	Flow depth on dry land (m)				
Velocity scenarios	Initial surface water elevation (m)	Pit water gauge	Highway 112 water gauges		Black Lake water gauges		
		# 01	# 04	# 06	# 02	# 03	# 08
Slow	150	167.0	-	-	-	-	-
	225	231.4	0.05	-	-	-	-
	230	236.0	1.0	-	-	-	-
	233	239.0	3.0	0.3	-	-	Almost
	235	241.0	3.2	0.5	-	-	1.0
Rapid	150	168.0	-	-	-	-	-
	195	214.3	Almost	-	-	-	-
	230	246.0	11.0	3.0	-	1.0	3.0
	233	248.3	12.3	3.6	-	2.7	4.5
	235	250.0	13.0	4.0	-	3.0	8.0
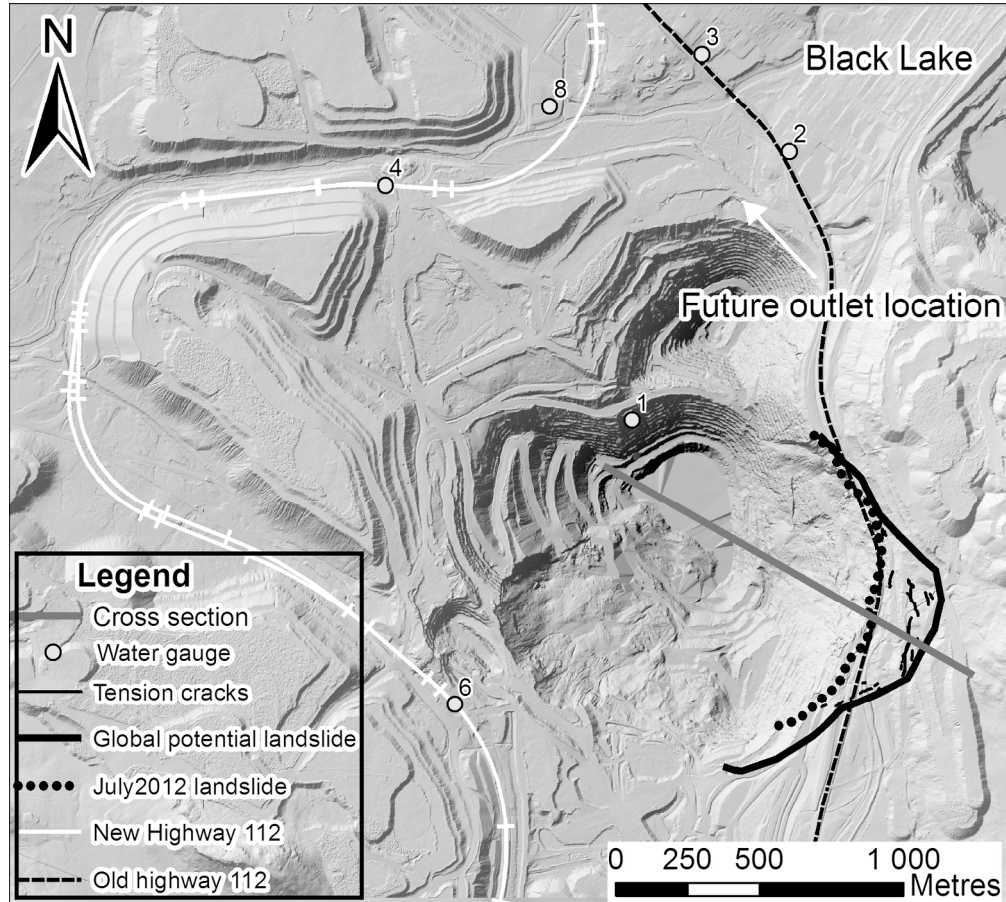
Fig. 1. Hillshade image derived from the DEM of the study area showing the main scarp location of the different mass movement episodes that occurred since 2010 on the perimeter of the abandoned open-pit mine located south of Black Lake. Location of the different numeric water gauges are also marked on the figure. In the inset is the location of the area, marked by a star.

163x146mm (300 x 300 DPI)

Fig. 2. Geometry of the Global rockslide scenario of 50 M m³. Three contour lines were added for elevations 150, 200 and 233 m.

130x148mm (300 x 300 DPI)
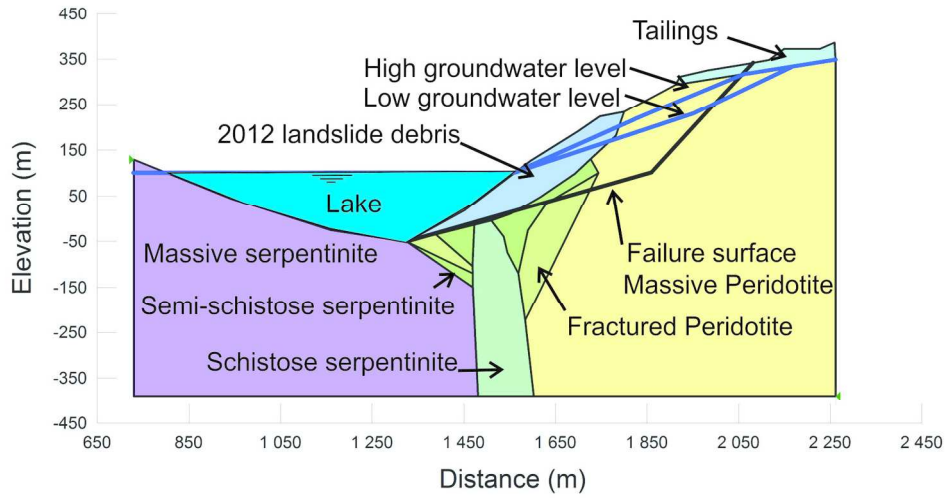
Fig. 3. Geological and geotechnical model used for the slope stability analysis. In this case, the water level is of 100 m.

165x96mm (300 x 300 DPI)
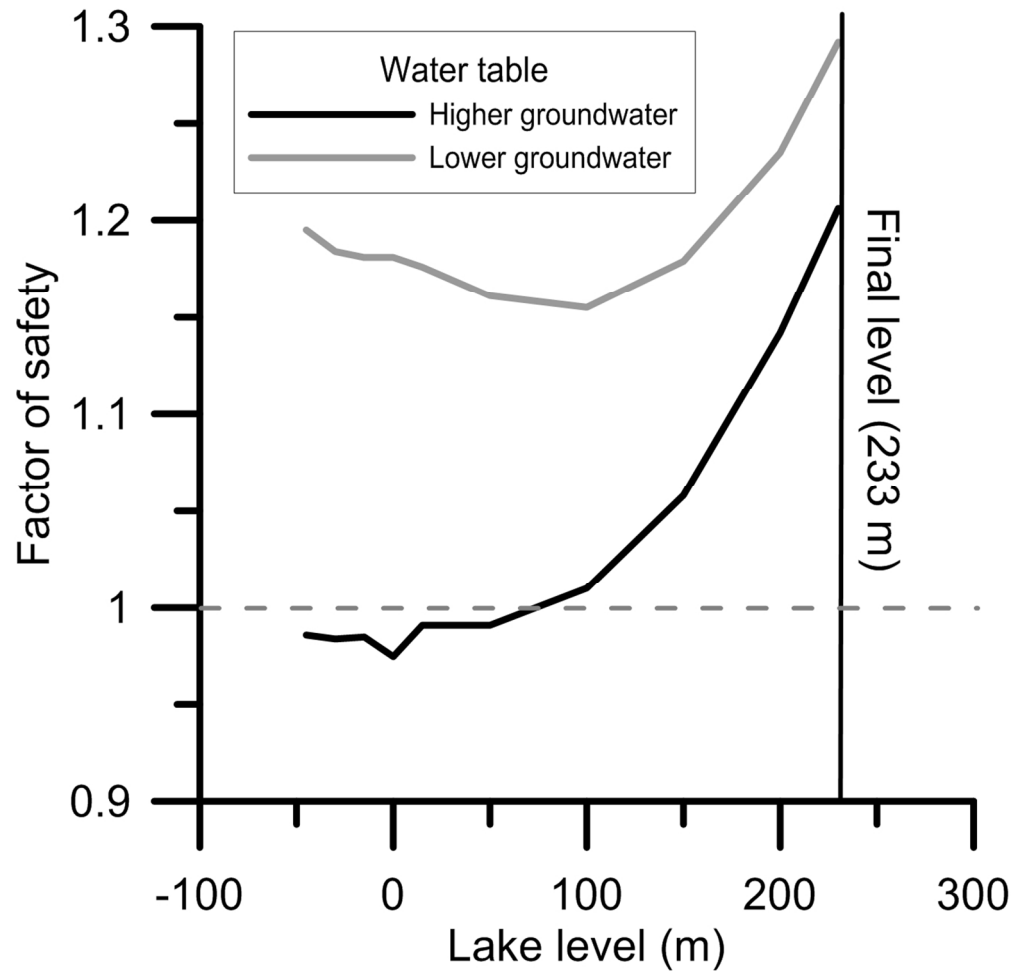
Fig. 4. Factor of safety evolution of the Global rockslide as a function of pit flooding for two different water table scenarios in the rock mass, illustrated on Fig. 2.
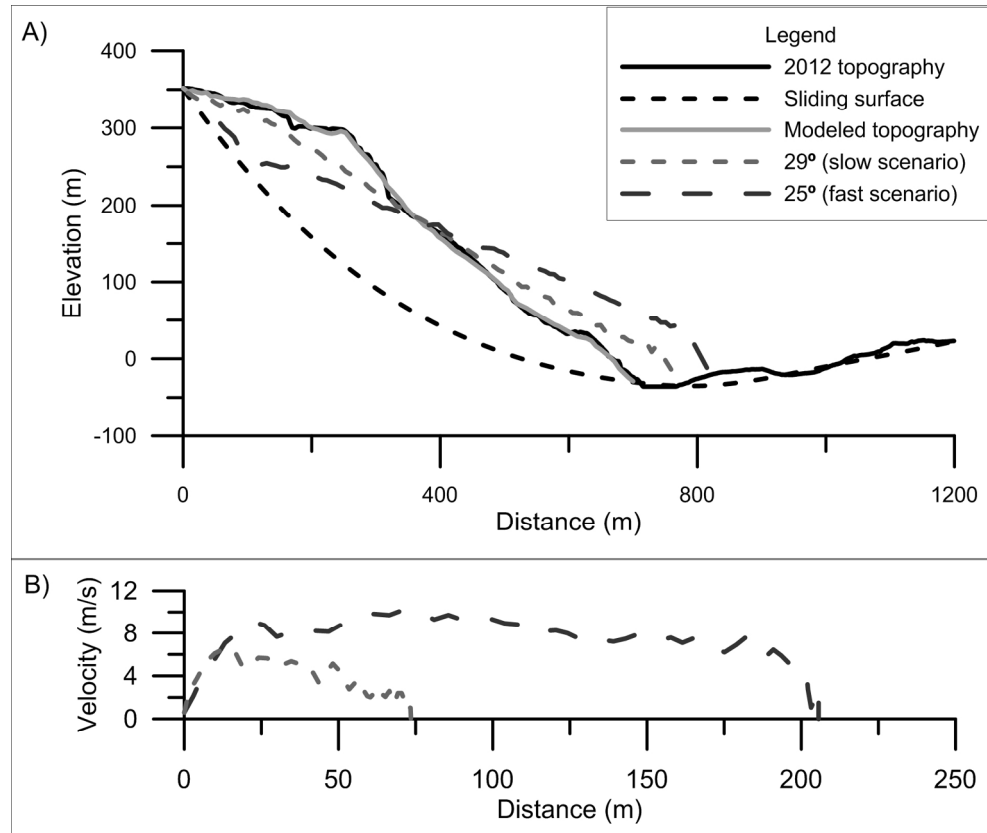
111x108mm (299 x 299 DPI)

Fig. 5. a) Used profiles for the Global rockslide NIS modelling with the spreading results from two different friction angles. The cross-section used for the 2D topographic profiles is shown in Fig. 1. b) Velocity evolution with center of mass traveled distance for the two velocity scenarios of the Global rockslide.

165x137mm (299 x 299 DPI)
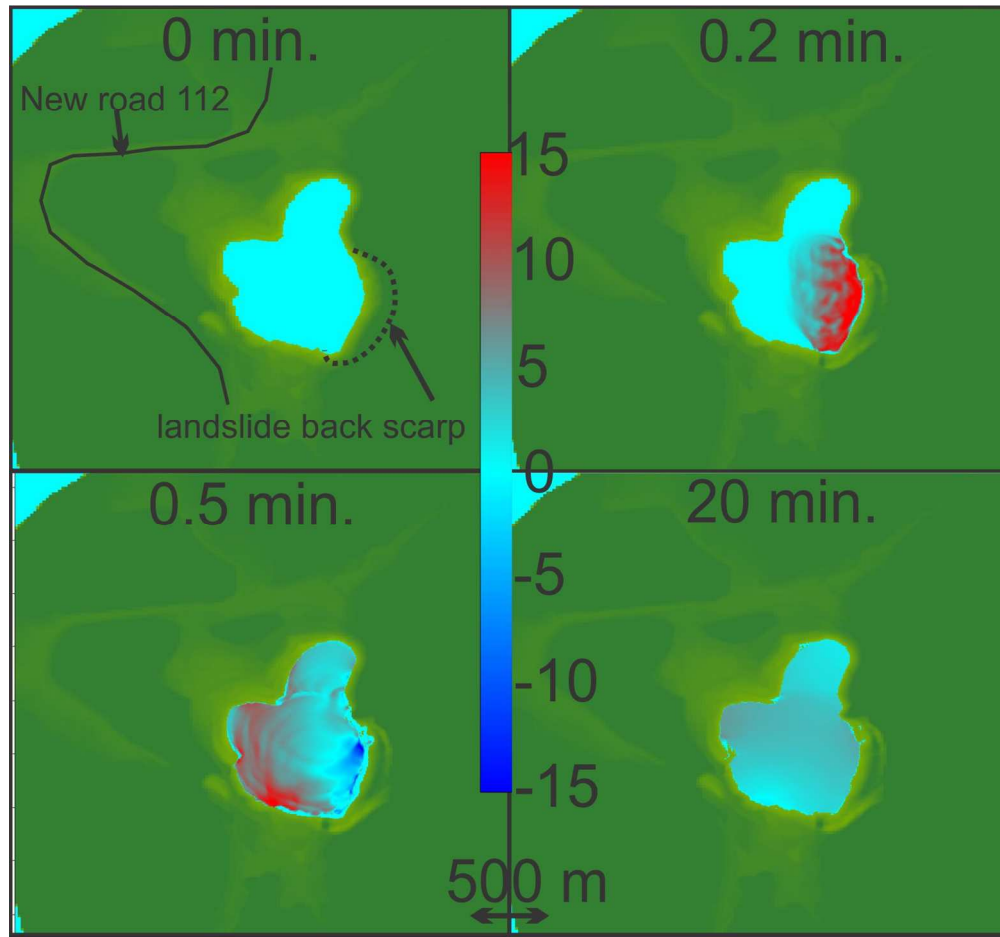
Fig. 6 : Plan view of the numerical modeling results of the global landslide, using rapid velocity scenario and an initial lake water level of 150 m. North is up.
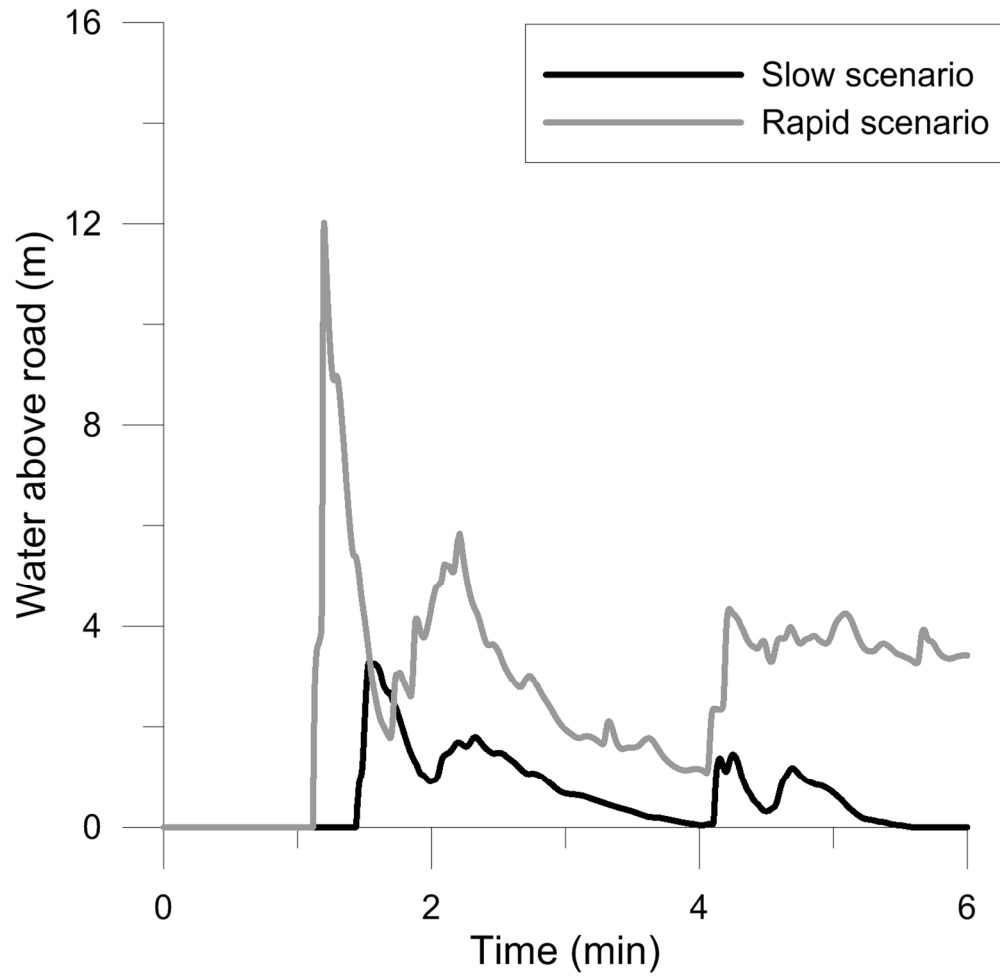
144x135mm (300 x 300 DPI)

Fig. 7. Water height above road (gauge 04) for the two velocity scenarios when the lake will be at its maximum water level (233 m) capacity (Global landslide).
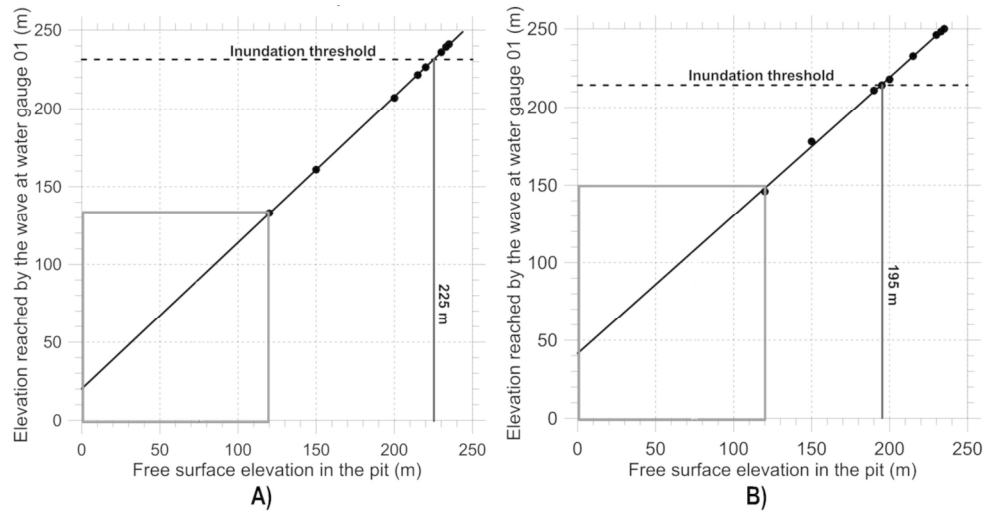
124x120mm (299 x 299 DPI)

Fig. 8. Maximal elevation reached by the wave in the main pit at water gauge 01 (Fig. 1) for different initial free surface elevation for the Global scenario and with the slow velocity profile in (a) and rapid velocity profile in (b). The red box delimits the zone where the factor of safety is lower than unity.
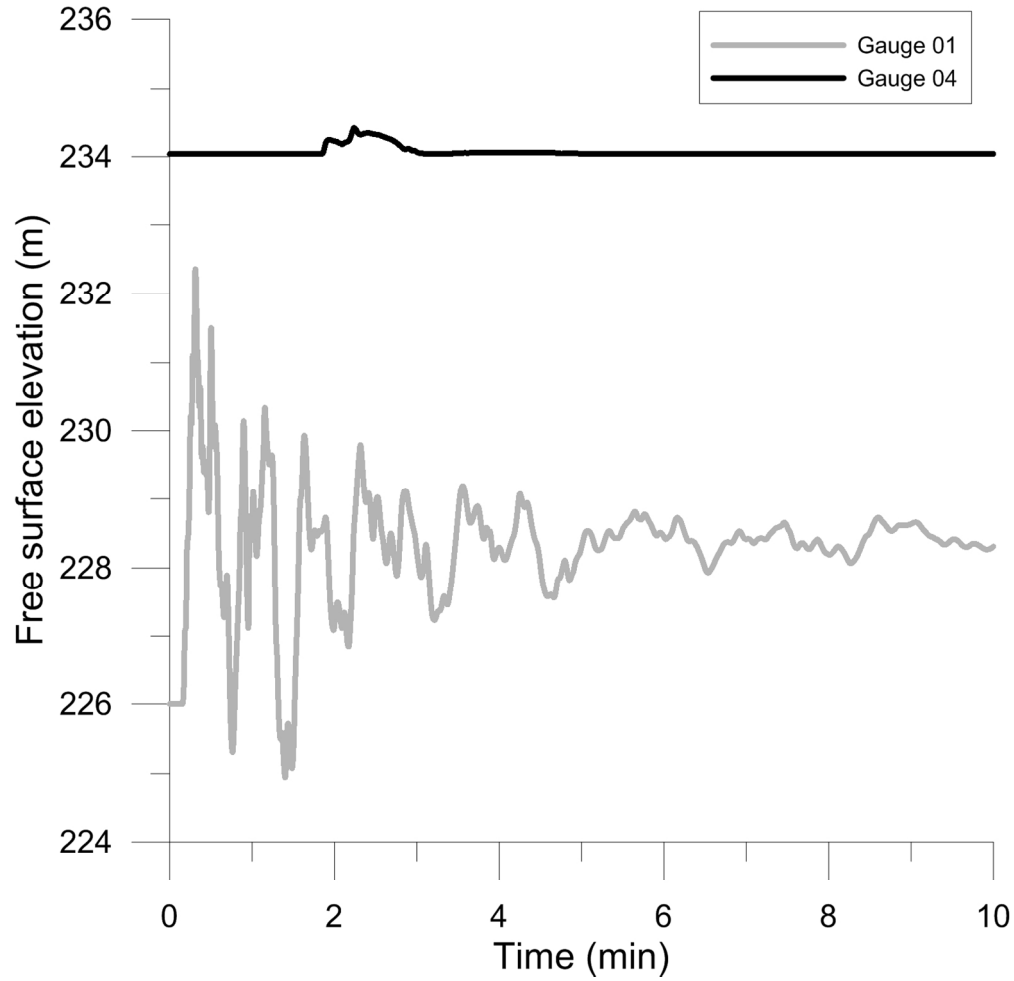
253x131mm (300 x 300 DPI)

Fig. 9. Results from the simulations with the slow velocity scenario, for gauges 01 and 04, when the lake will be filled up to an elevation of 226 m (Global landslide).

134x130mm (299 x 299 DPI)